Electronic Supplementary Material (ESI) for Soft Matter.

# Supporting Information

# Polymer ligand binding to surface-immobilized gold nanoparticles: A fluorescence-based study on the adsorption kinetics

*Julian Sindram*[a]* *and Matthias Karg*[a]

[a]Institut für Physikalische Chemie I: Kolloide und Nanooptik, Heinrich-Heine-Universität
Düsseldorf, Universitätsstr. 1, 40225 Düsseldorf, Germany

## Measurement setup

**Figure S1** shows a top-view sketch of the general experiment layout for fluorescence measurements. The experiments are performed with standard fluorescence cuvettes (1 cm x 1 cm). The substrate faces the emission arm of the spectrometer to minimize reflection/scattering of the excitation beam by the substrate. The stirrer bar is at the bottom of the cuvette and outside the excitation and detection light paths.

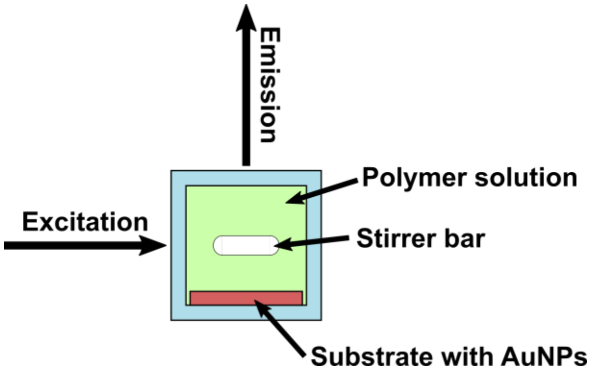

**Figure S1:** Sketch of the experiment layout for fluorescence measurements to study the ligand binding kinetics. The excitation and the emission optics are both focused on the center of the quartz cuvette.

## Characterization of substrates with immobilized gold nanoparticles

The gold nanoparticle distribution and the homogeneity of the surface coverage on the glass substrates was investigated by AFM. **Figures S2-6** show AFM height images of two scan areas on five different substrates. The corresponding particle number densities, determined by automated image analysis (ImageJ) are given above the individual scans. Particles at the image edges were not included. The particles are randomly distributed and there are no clusters. There is only little fluctuation between particle number densities from the different measurements, confirming the good consistency and reproducibility of our deposition method.

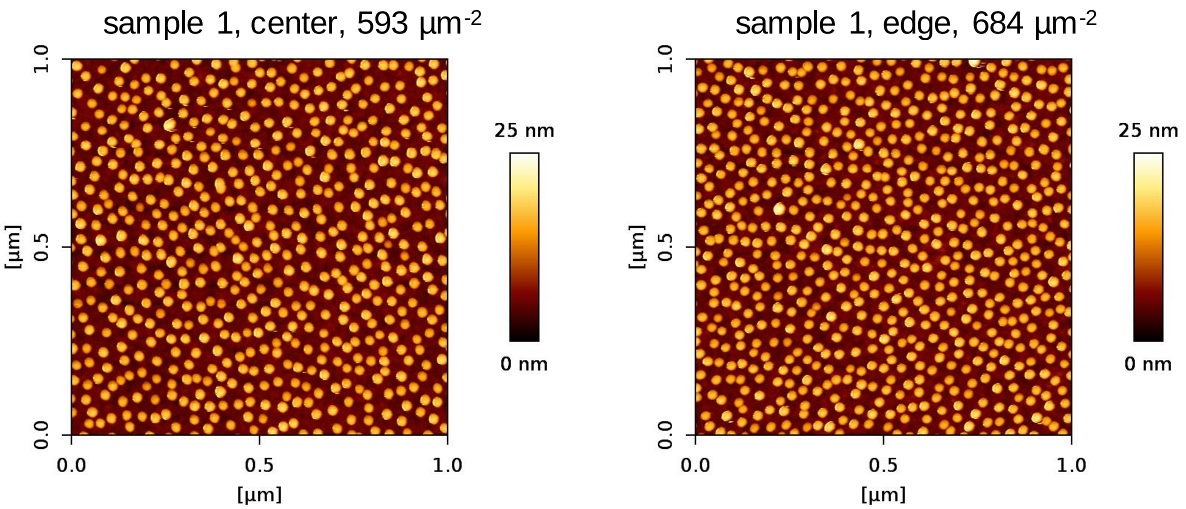
sample 1, center, 593 µm$^{-2}$

sample 1, edge, 684 µm$^{-2}$

**Figure S2:** AFM height images of the first sample of gold nanoparticles immobilized on amine-functionalized glass substrates measured in intermittent contact mode. The corresponding particle number densities are given in the image titles above each AFM image.

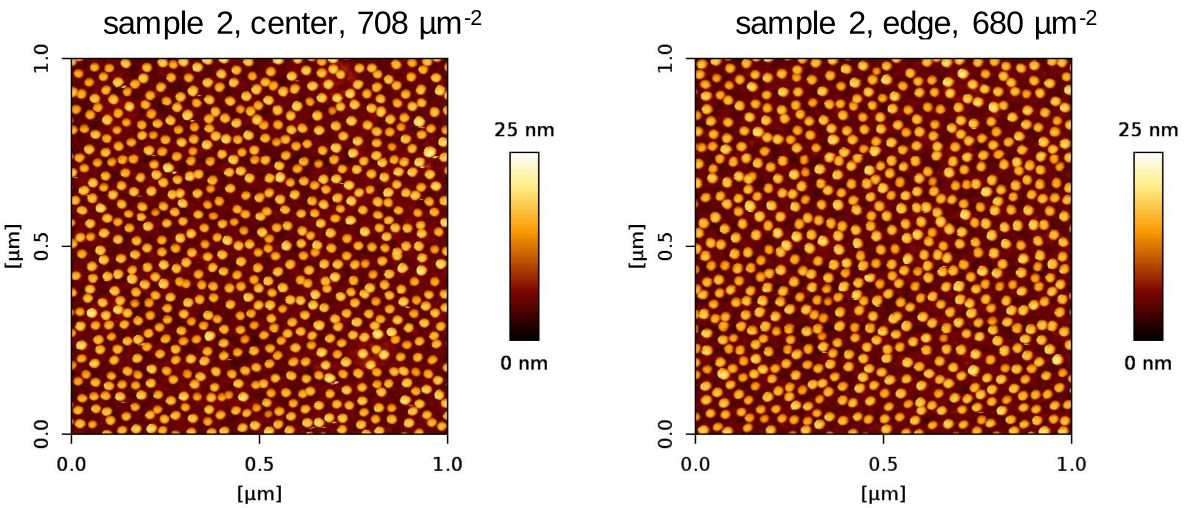
sample 2, center, 708 µm$^{-2}$

sample 2, edge, 680 µm$^{-2}$

**Figure S3:** AFM height images of the second sample of gold nanoparticles immobilized on amine-functionalized glass substrates measured in intermittent contact mode. The corresponding particle number densities are given in the image titles above each AFM image.

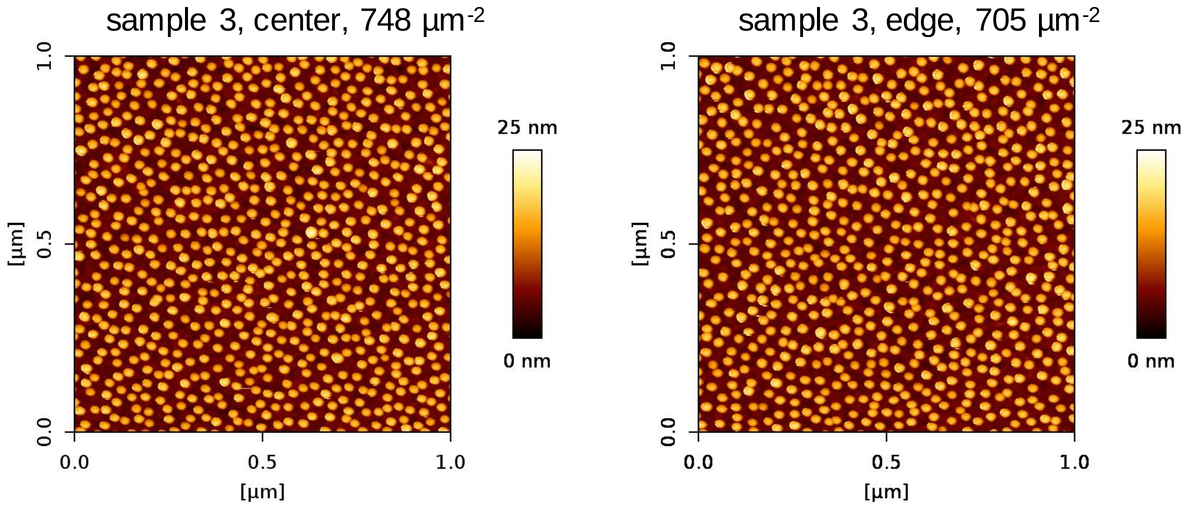
sample 3, center, 748 µm$^{-2}$

sample 3, edge, 705 µm$^{-2}$

**Figure S4:** AFM height images of the third sample of gold nanoparticles immobilized on amine-functionalized glass substrates measured in intermittent contact mode. The corresponding particle number densities are given in the image titles above each AFM image.

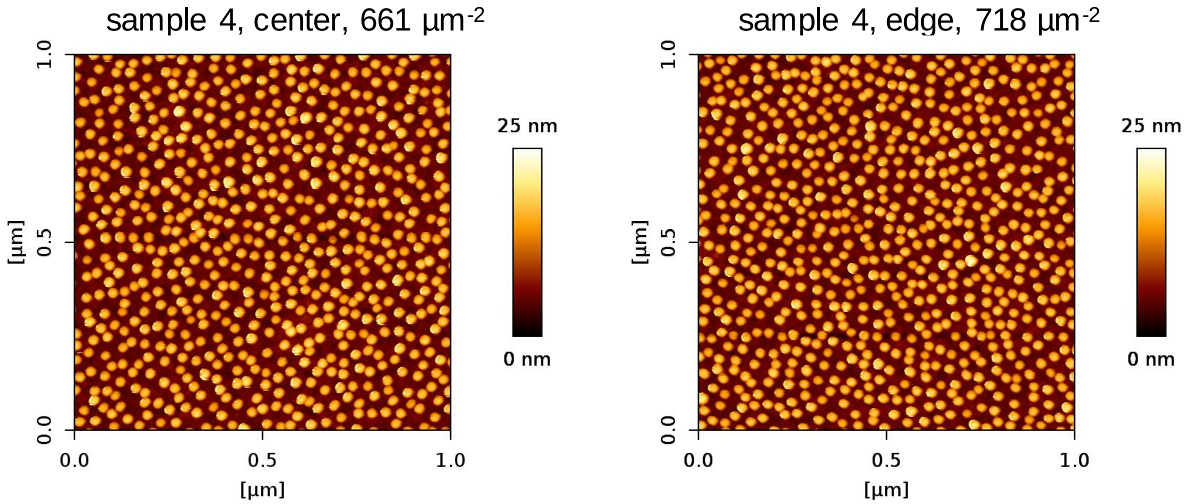
sample 4, center, 661 µm$^{-2}$

sample 4, edge, 718 µm$^{-2}$

**Figure S5:** AFM height images of the fourth sample of gold nanoparticles immobilized on amine-functionalized glass substrates measured in intermittent contact mode. The corresponding particle number densities are given in the image titles above each AFM image.

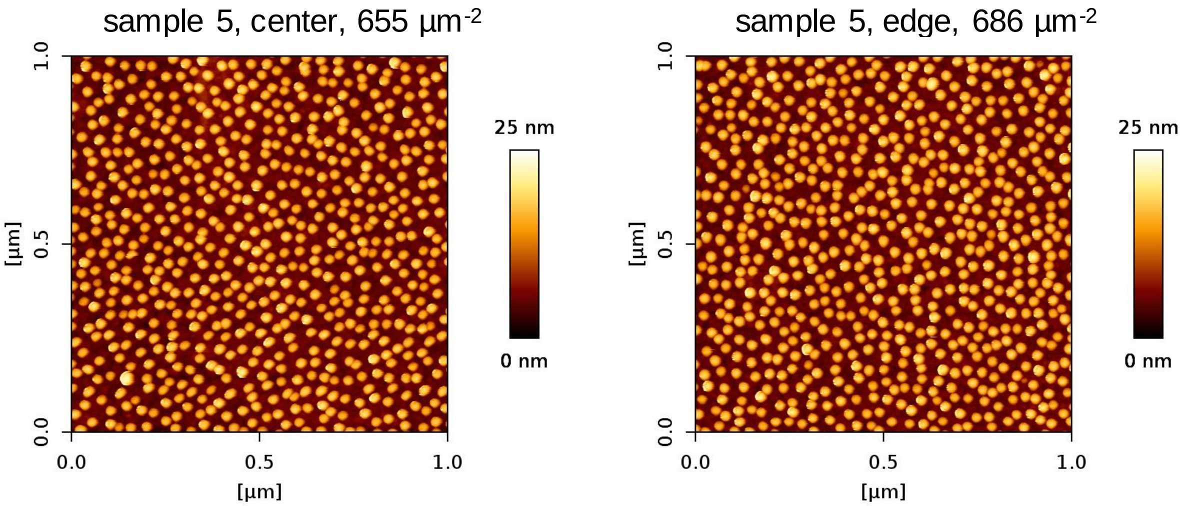

**Figure S6:** AFM height images of the fifth sample of gold nanoparticles immobilized on amine-functionalized glass substrates measured in intermittent contact mode. The corresponding particle number densities are given in the image titles above each AFM image.

In the following, we would like to prove the absence of any pronounced order in the arrangement of the gold nanoparticles on the substrates. We use the height image for **sample 1, center** as an example. **Figure S7** shows the single point positions from the AFM image in **Figure S2** and the corresponding FFT. Both operations (find maxima/single point output and FFT) were performed in ImageJ. The FFT shows no features apart from a dark circle in the center, related to the closest possible interparticle distance on the order of the particle diameter. Otherwise, there are no indications for a preferred interparticle distance (concentric rings) or periodically order arrangement (peaks) in the FFT. Therefore, the particles are randomly distributed.

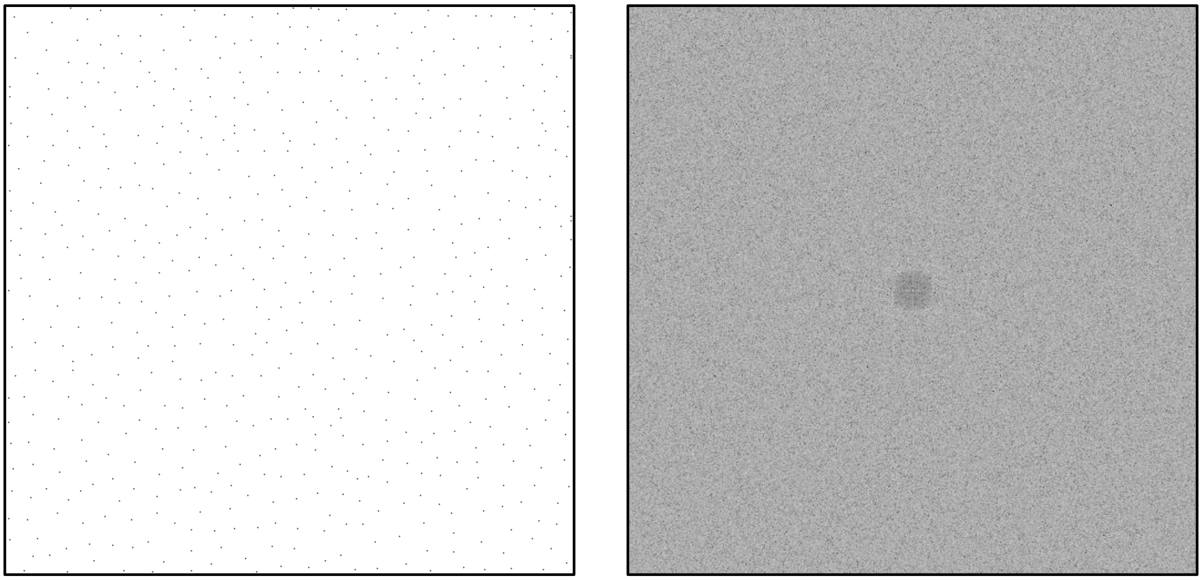

**Figure S7:** Single point particle positions (left) and corresponding FFT (right) for sample 1, center. The FFT exhibits no features corresponding to periodic structuring of the particles.

## Characterization of substrates after ligand binding experiments

In the following investigate the particle arrangement and number density after the ligand binding experiments. This is to confirm that the particles remain attached to the substrate surface even after plasma cleaning and prolonged immersion in water and DMF. **Figures S8-S10** show AFM height and phase images for substrates after ligand binding experiments with the three different polymer ligands used in this work. The particle arrangement is similar in appearance to the as-prepared substrates. The particle number densities are in the range seen for the as-prepared substrates. We can therefore conclude that the particles do not detach from the substrates during the kinetics experiments.

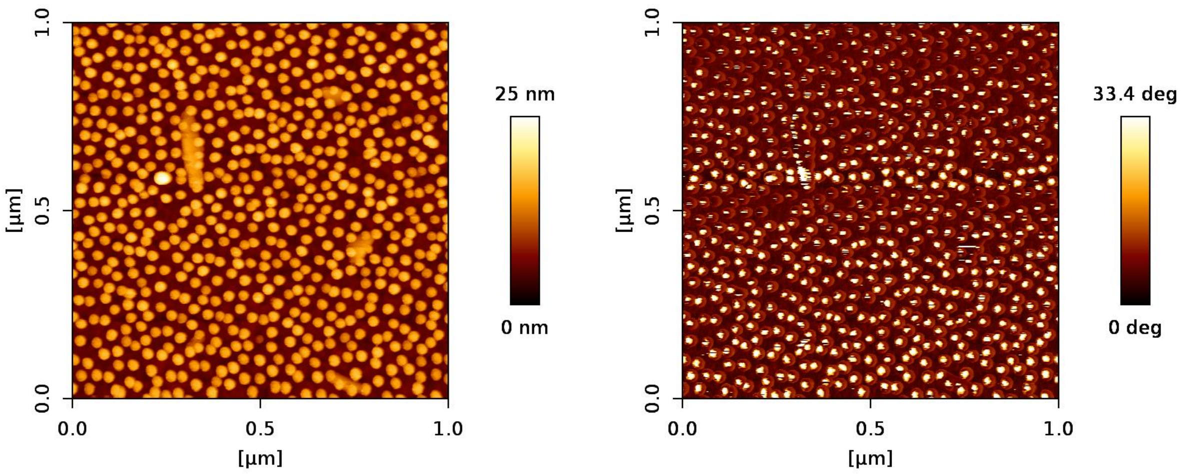

**Figure S8:** AFM height (left) and phase image (right) of gold nanoparticles of a sample after the kinetics experiment using ligand with a molecular weight of 6.5 kg/mol. The corresponding particle number density is 643 µm$^{-2}$.

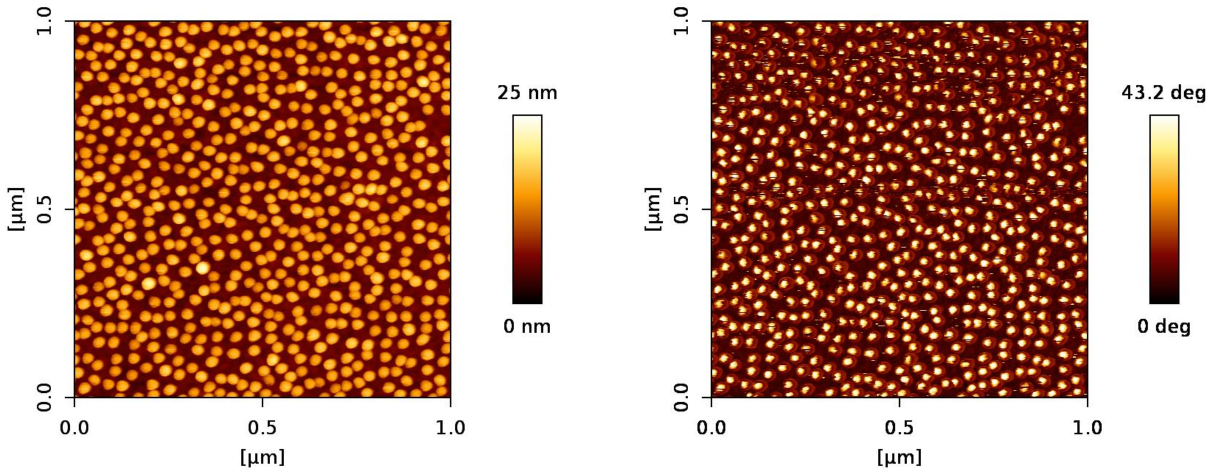

**Figure S9:** AFM height (left) and phase image (right) of gold nanoparticles of a sample after the kinetics experiment using ligand with a molecular weight of 21 kg/mol. The corresponding particle number density is 681 µm$^{-2}$.

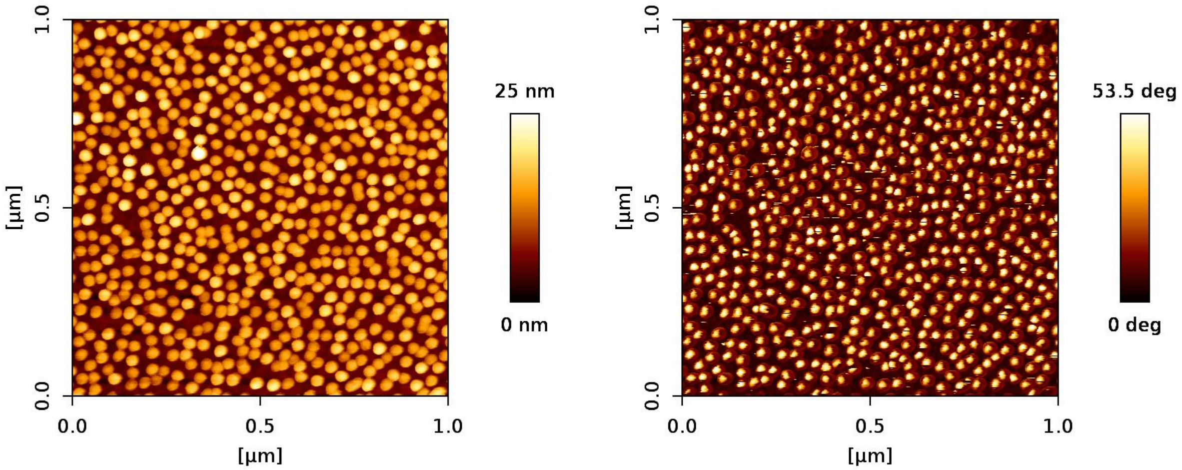

**Figure S10:** AFM height (left) and phase image (right) of gold nanoparticles of a sample after the kinetics experiment using ligand with a molecular weight of 33 kg/mol. The corresponding particle number density is 675 µm$^{-2}$.

## AFM data analysis for measurements in QI mode

We use high resolution force mapping (QI mode) to examine the morphology of the substrates supported gold nanoparticles after the ligand binding experiments. A force curve is obtained for each pixel and analyzed using the batch processing function of the JPK Data Processing software (v.6.1.142). The analysis process is shown step-by-step in **Figures S11-S15**.

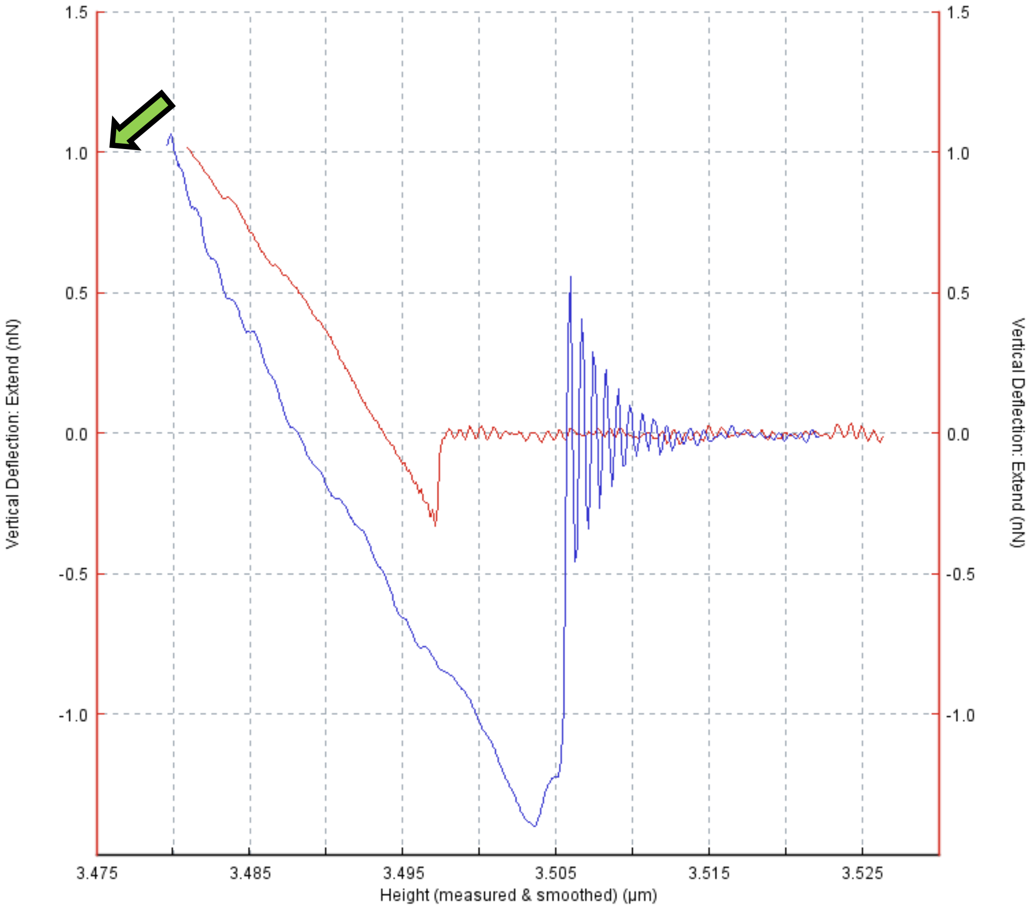

**Figure S11:** A typical baseline-corrected force curve. The force is plotted against the height. The red line represents the extension, the blue line represents the retraction. The setpoint force (green arrow) for the measurement was 1 nN. Note the oscillations in the retraction curve after the minimum (adhesion) has been passed.

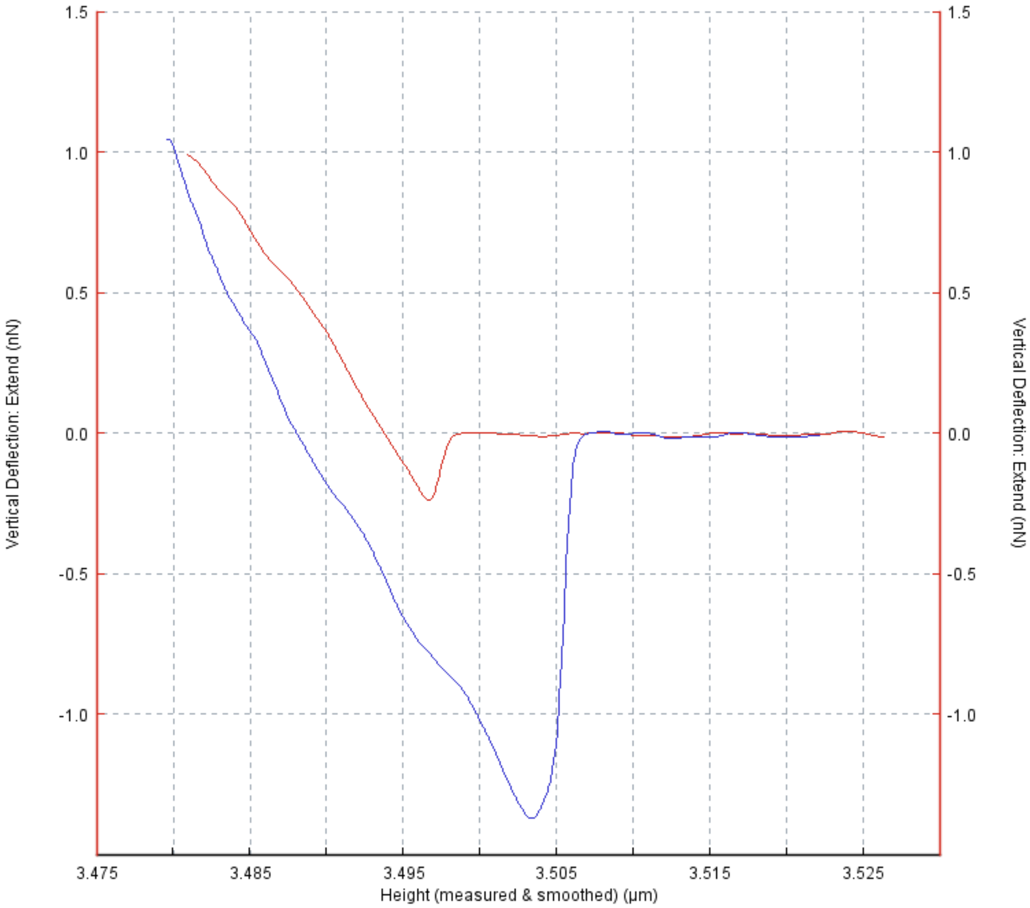

**Figure S12:** The noise is reduced by a Gaussian filter.

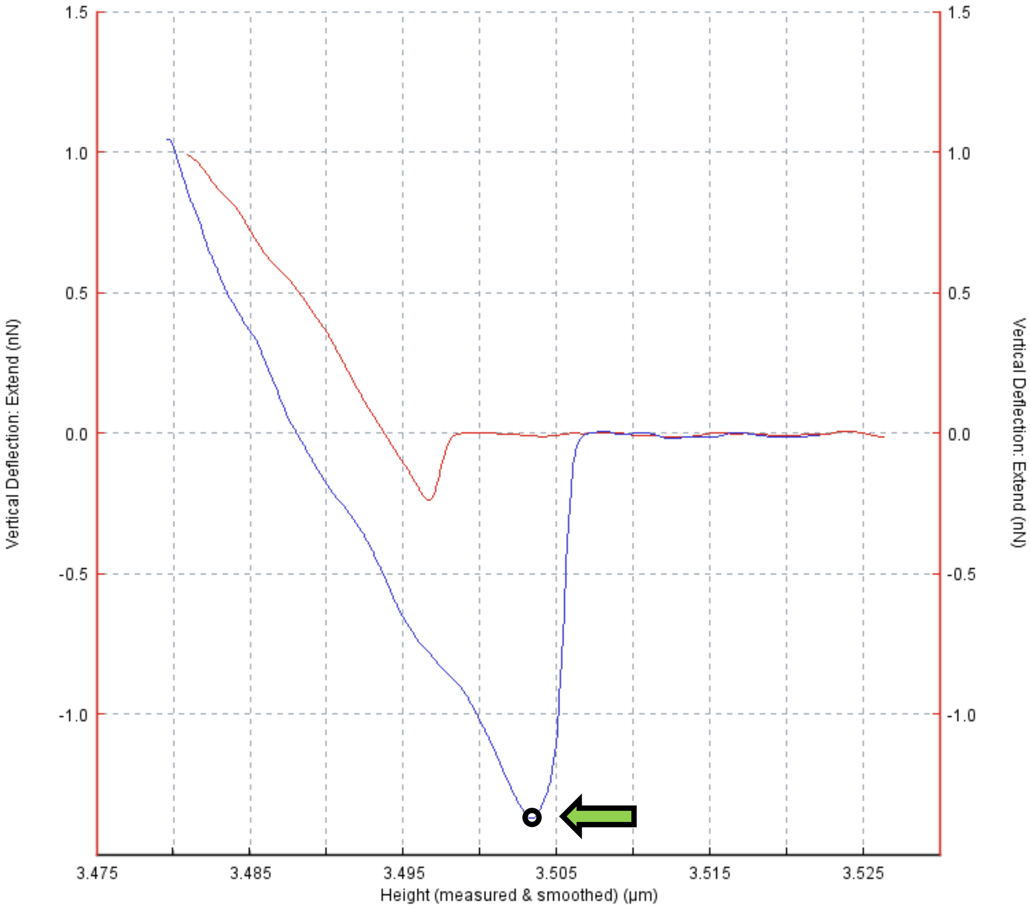

**Figure S13:** The adhesion force is determined from the minimum of the retraction curve.

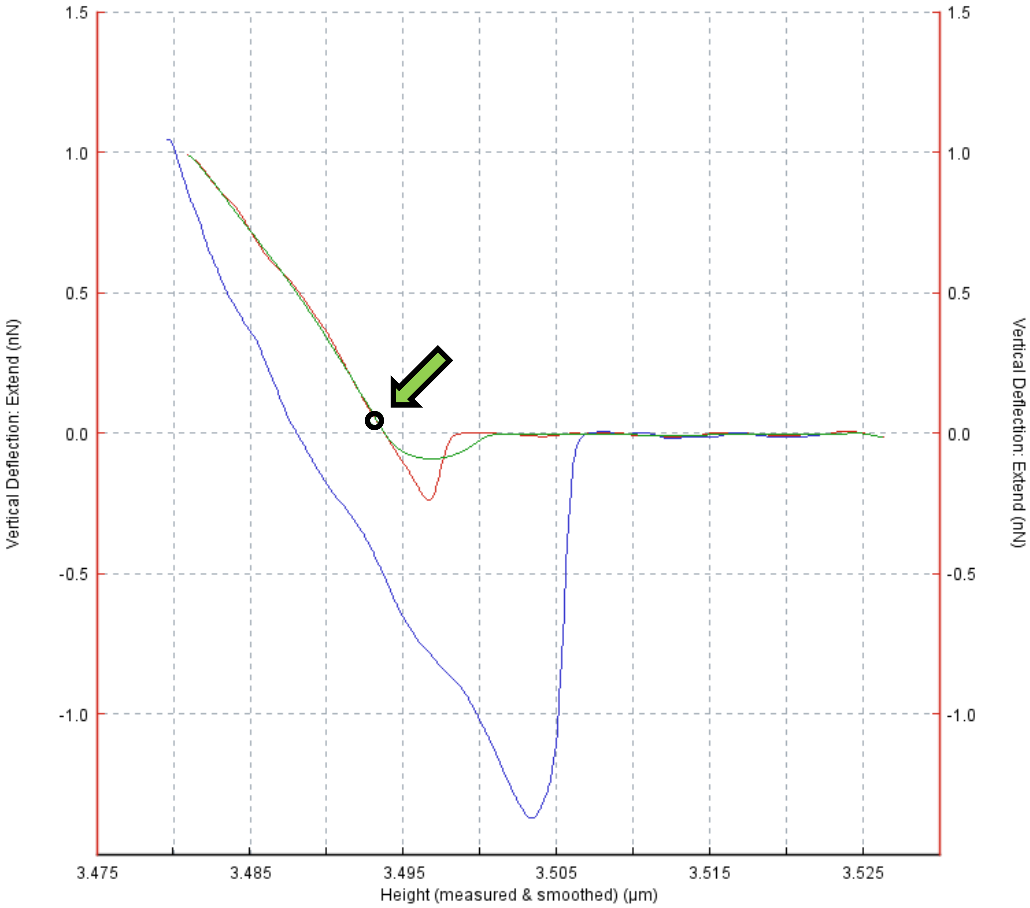

**Figure S14:** The extension curve is fitted (green line) and the height (*x* axis) at a chosen reference force (*y* axis) is interpolated. Here, the reference force is 50 pN.

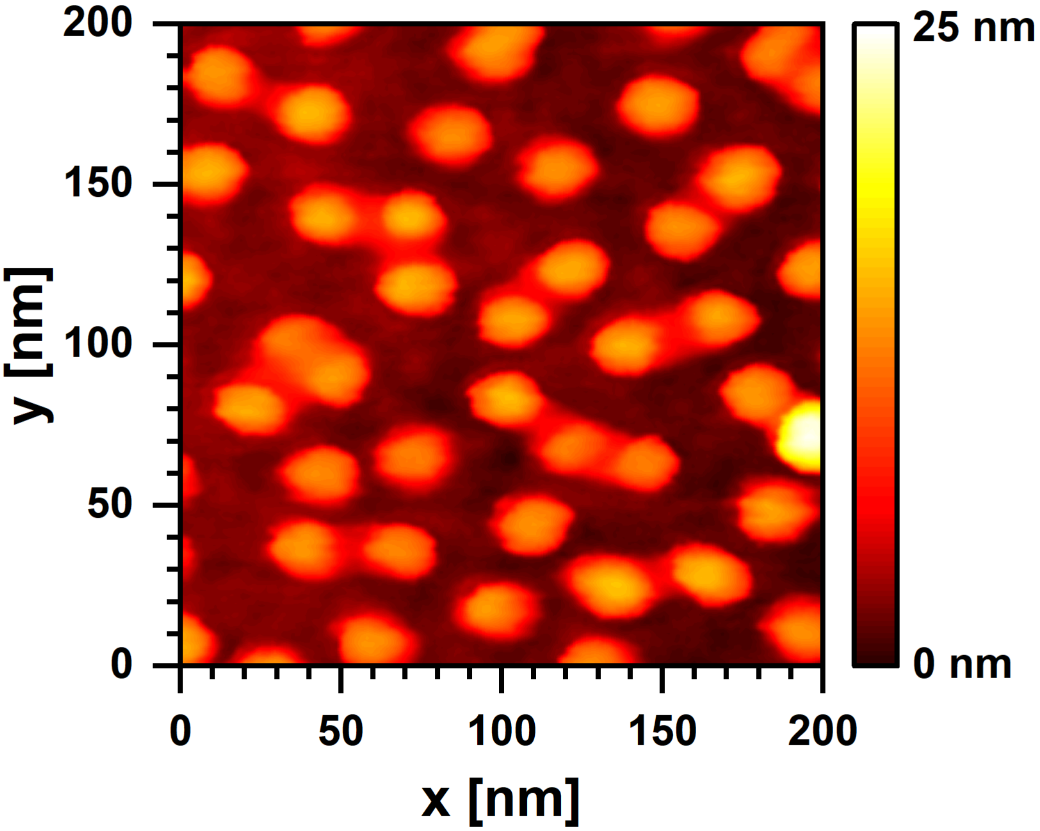

**Figure S15:** Images are constructed from the height and adhesion information. Here, the resulting height image for a sample after the ligand binding experiment (33 kg/mol ligand) is shown as an example.

The height and adhesion images for samples of an as-prepared substrate and after ligand binding with ligand molecular weights of 6.5, 21, and 33 kg/mol respectively are shown in **Figures S16-S19**. The height and adhesion images of as-prepared substrate-supported AuNPs show well defined particle outlines, whereas the images of samples after ligand binding experiments show more diffuse outlines. There appears to be a corona around the particles that has a low height profile but distinctly different adhesion characteristics than the substrate. We conclude that this corona is polymer bound to the particle surface. The clear localization of the polymer around the particles is further evidence for the absence of non-specific adsorption of polymer to the substrate.

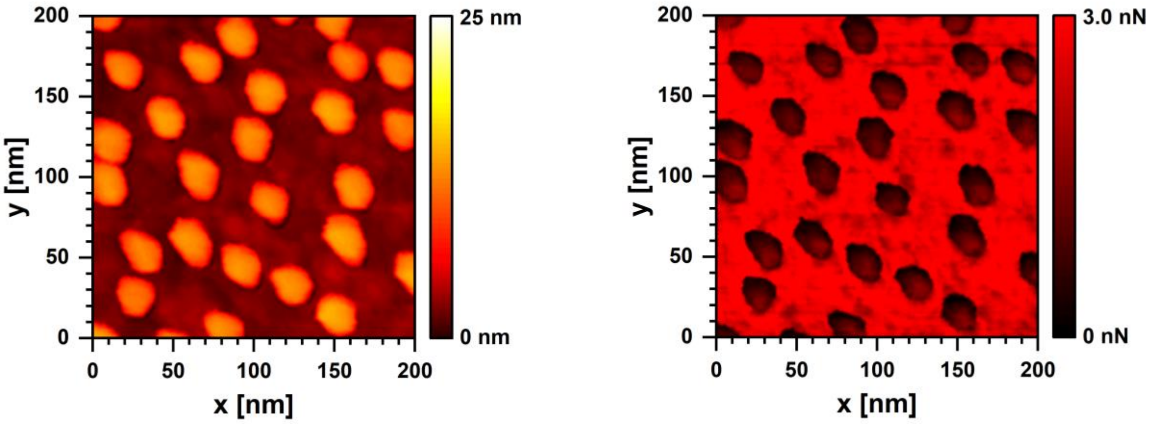

**Figure S16:** AFM height (left) and adhesion (right) image of an as-prepared sample of substrate-supported AuNPs.

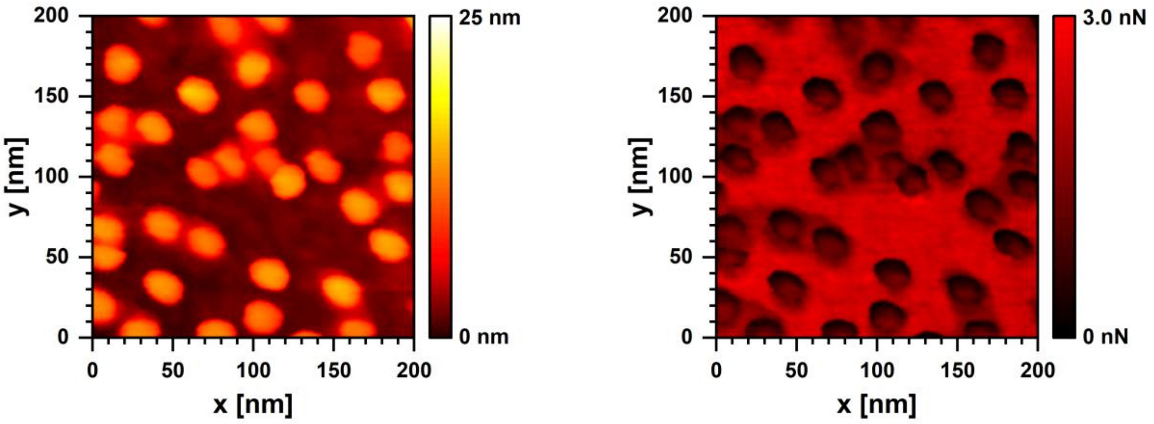

**Figure S17:** AFM height (left) and adhesion (right) image of a sample of substrate-supported AuNPs after the ligand binding experiment using a polymer with a molecular weight of 6.5 kg/mol.

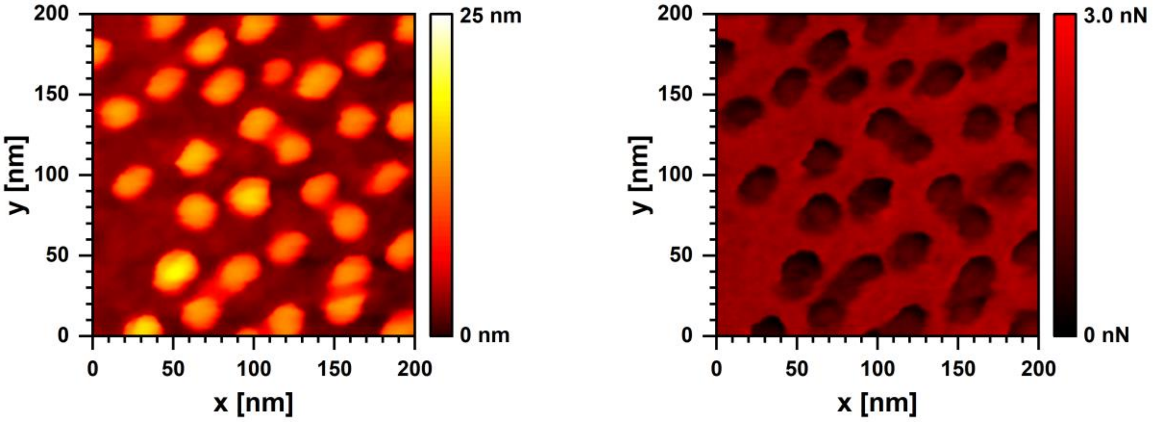

**Figure S18:** AFM height (left) and adhesion (right) image of a sample of substrate-supported AuNPs after the ligand binding experiment using a polymer with a molecular weight of 21 kg/mol.

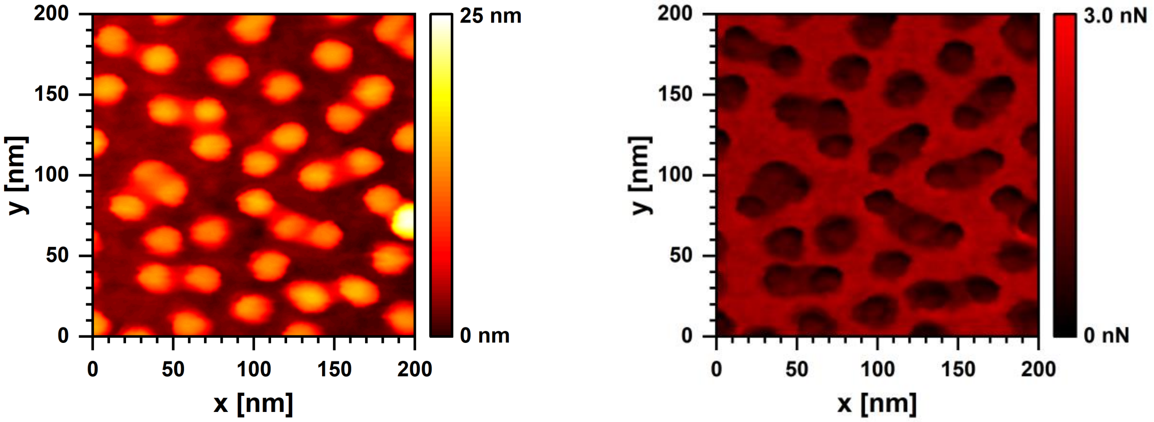

**Figure S19:** AFM height (left) and adhesion (right) image of a sample of substrate-supported AuNPs after the ligand binding experiment using a polymer with a molecular weight of 33 kg/mol.

### Non-specific adsorption on APTMS-functionalized substrates

The importance of plasma deactivation of the substrates with immobilized gold nanoparticles becomes apparent when no gold nanoparticles are present. **Figure S20** shows representative curves for the fluorescence intensity measured for an as-prepared APTMS functionalized substrate and a plasma deactivated APTMS functionalized substrate. There is a significant decrease in fluorescence intensity for the as-prepared substrate, indicating non-specific adsorption of polymer ligand. Hence, plasma deactivation is necessary to avoid interference of the non-specific adsorption with the specific adsorption on the nanoparticle surface. The deactivation can also be achieved by chemical capping of the free amine groups with organic acid anhydrides, such as succinic and acetic anhydride.

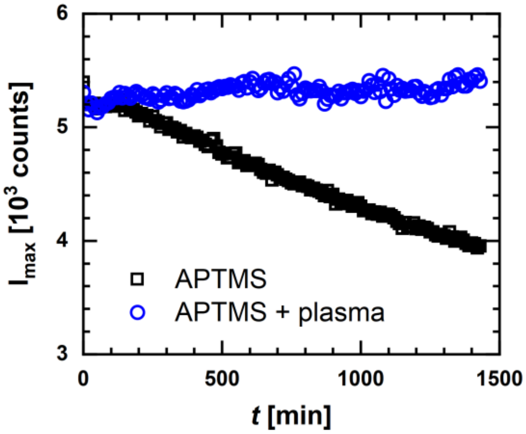

**Figure S20:** Representative intensity-time curves for APTMS functionalized glass before and after plasma deactivation.

### Considerations regarding the equilibrium state during kinetic experiments

The equilibrium state, i.e. the plateau grafting density on the particle surface, gives insight into the driving force of the adsorption and desorption processes. For this, we consider the theoretical dimensions of a brush formed on the AuNP surface in relation to the measured chain dimensions in solution. We obtain the hydrodynamic radius, $R_h$, of the chains from DLS measurements. We convert $R_h$ into the radius of gyration, $R_g$, using $R_g \approx 1.505\ R_h$.[1] The double logarithmic plot of $R_g$ in relation to the number of monomer units, $N$, is shown in **Figure S21.**

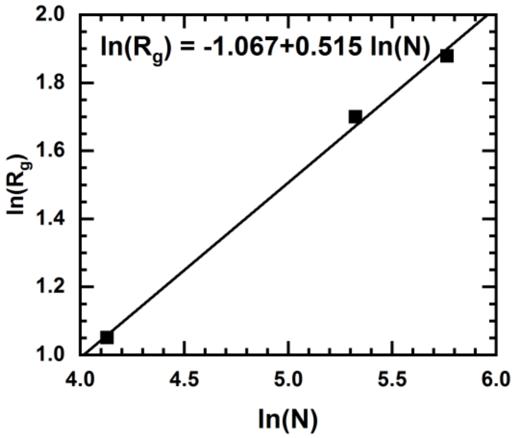

**Figure S21:** Double logarithmic plot showing the scaling relation for the radius of gyration in relation to the degree of polymerization. The equation of the fit is given.

From the fit we obtain the scaling relation given in **Equation S1**. Here, $l$ is the statistical segment length per monomer unit and $\nu$ is the scaling exponent.[2] The slope of the fit resembles the scaling exponent, whereas the intercept is the natural logarithm of the product of the statistical length and the numerical prefactor.

$$R_g = \frac{1}{\sqrt{2(1+\nu)(2\nu+1)}} lN^{\nu} = 0.403 \cdot 0.85 \text{ nm } N^{0.515} \approx \frac{1}{\sqrt{6}} \cdot 0.85 \text{ nm } N^{0.5} \tag{S1}$$

PS dissolved in DMF at 20 C shows almost ideal chain behavior ($\nu = 0.5$). For the height, $h$, of the polymer brush formed on the particle surface, we assume scaling according to the semi-dilute curved brush model in θ conditions, shown in **Equation S2**.[3] Here, $\sigma^* = \sigma\ l^2$ is the reduced grafting density.

$$h \approx lN^{0.5} \sigma^{*0.25} \tag{S2}$$

We estimate that approximately half the particle surface is accessible to the ligands and calculate $\sigma^*$ according to **Equation S3**. The real $\sigma^*$ can be assumed to be proportional to this value. $\overline{f_\infty}$ is the average number of chains per particle in equilibrium and $r_{Au}$ is the radius of the gold nanoparticles.

$$\sigma^* \approx \frac{\overline{f_\infty}}{2\pi {r_{Au}}^2} l^2 = 3.1 \cdot 10^{-3}\, \overline{f_\infty} \tag{S3}$$

Using $l = 0.85$ nm from the scaling in solution, the theoretical brush height can then be calculated by:

$$h \approx 0.85 \text{ nm } N^{0.5}\left(3.1 \cdot 10^{-3} \overline{f_\infty}\right)^{0.25} \tag{S4}$$

If we now divide $h$ by the experimental $R_g$, we obtain a dimensionless chain stretching factor for the elongation of the polymer chain in the brush:

$$\frac{h}{R_g} = \frac{0.85 \text{ nm } N^{0.5}\left(3.1 \cdot 10^{-3} \overline{f_\infty}\right)^{0.25}}{R_g} \tag{S5}$$

The calculated stretching factors are listed in **Table S1**. Although the exact factor may differ from these values, we can expect that the chains are stretched to a similar degree. It therefore seems reasonable to assume that the equilibrium of the ligand binding is determined by the free energy required to stretch the chains in relation to the free energy gained by chain adsorption.

**Table S1:** Calculated chain stretching factor between theoretical polymer brush height and the radius of gyration in solution.

| Ligand | $\overline{f_\infty}$ | $R_g$ [nm] | $h/R_g$ |
|---|---|---|---|
| $PS_{6.5}$ | 45 ± 3 | 2.9 | 1.4 ± 0.1 |
| $PS_{21}$ | 28 ±4 | 5.5 | 1.2 ± 0.2 |
| $PS_{33}$ | 29 ± 2 | 6.5 | 1.3 ± 0.1 |

## REFERENCES

1. Haydukivska, K.; Blavatska, V.; Paturej, J., Universal size ratios of Gaussian polymers with complex architecture: radius of gyration vs hydrodynamic radius. *Scientific Reports* **2020,** *10* (1), 14127.

2. Akcasu, A. Z.; Han, C. C., Molecular Weight and Temperature Dependence of Polymer Dimensions in Solution. *Macromolecules* **1979,** *12* (2), 276-280.

3. Lo Verso, F.; Yelash, L.; Egorov, S. A.; Binder, K., Effect of the solvent quality on the structural rearrangement of spherical brushes: coarse-grained models. *Soft Matter* **2012,** *8* (15), 4185-4196.